AGU PUBLICATIONS

[Earth and Space Science]

Supporting Information for

[Radar interferometry offers new monitoring approach for critical flood control infrastructure]

[K. An[1], C. E. Jones[2], D. P. S. Bekaert[2] and V. Bennett [3]]

[[1] Department of Geography, University of California, Los Angeles, Los Angeles, CA 90095, USA.

[2] Jet Propulsion Laboratory, California Institute of Technology, Pasadena, CA 91109, USA.

[3] Department of Civil and Environmental Engineering, Rensselaer Polytechnic Institute, Troy, NY 12180, USA.]

Contents of this file

Introduction

The original raw GPS time series is shown for all three stations on Sherman Island, as well as a schematic of the GPS data conversion to the line-of-sight. Overview figures of vertical velocity and vertical velocity uncertainty are provided for the major Delta islands. In addition, a figure on the sensitivity analysis between the InSAR and lidar datasets is shown. An example of how the levee oriented moving window was generated is also shown. Lastly, 20 more examples of historic levee breaks are included which exceeded space in the paper.]

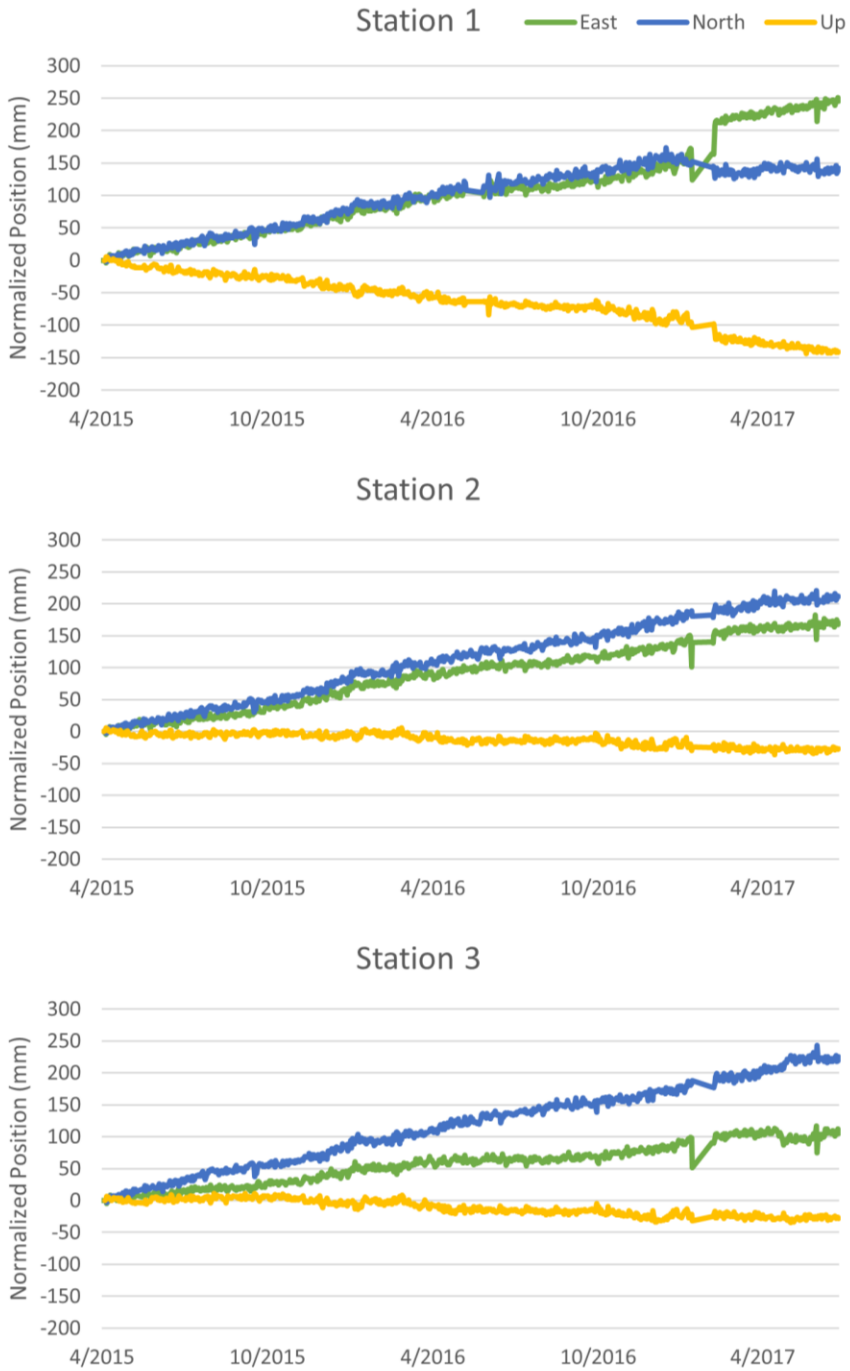

Figure S1. Original GPS time series. Raw time series (including data jumps) for the Sherman test site stations (locations shown in Fig. 2C). Positional change is normalized to the first data entry for visualization.

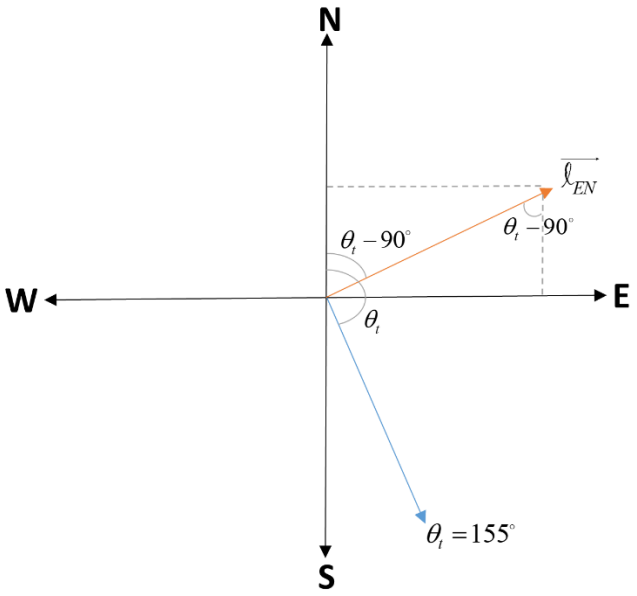

$$\ell_E = \ell_{EN}\sin(\theta_t - 90^\circ)$$
$$\ell_N = \ell_{EN}\cos(\theta_t - 90^\circ) \quad (1)$$

$$\hat{\ell} = \frac{\vec{\ell}}{\ell}$$
$$\hat{\ell} = -\cos\theta_i\hat{U} + \sin\theta_i\cos(\theta_t - 90^\circ)\hat{N} + \sin\theta_i\sin(\theta_t - 90^\circ)\hat{E} \quad (2)$$
$$\vec{\ell} = -\ell\cos\theta_i\hat{U} + \ell\sin\theta_i\cos(\theta_t - 90^\circ)\hat{N} + \ell\sin\theta_i\sin(\theta_t - 90^\circ)\hat{E}$$

$$\vec{d}_{GPS} = d_U\hat{U} + d_N\hat{N} + d_E\hat{E}$$
$$\vec{d}\cdot\hat{\ell} = -[d_U(-\cos\theta_i) + d_N\sin\theta_i\cos(\theta_t - 90^\circ) + d_E\sin\theta_i\sin(\theta_t - 90^\circ)] \quad (3)$$

Figure S2. GPS-LOS conversion. A schematic of the projected east-north component for UAVSAR flight line 15502 where θ_t is the track angle from north and $\overrightarrow{\ell_{EN}}$ is the east-north vector. Eq. 1 shows the individual east and north components in terms of the east-north vector and the track angle. Eq. 2 solves for the unit vector $\hat{\ell}$ by dividing the vector $\vec{\ell}$ by its length ℓ. The unit vector is shown in terms of its east, north, and up vectors where θ_i is the incidence angle. Eq. 3 shows the GPS displacement vector in terms of its east, north, and up components. The dot product between this displacement vector and the unit vector is solved to convert the GPS positions to the UAVSAR line-of-sight displacements. A final negative is taken of this equation because the GIAnT program assigns the look direction as positive looking up from the target. The converted LOS values are shown in Fig. 2E.

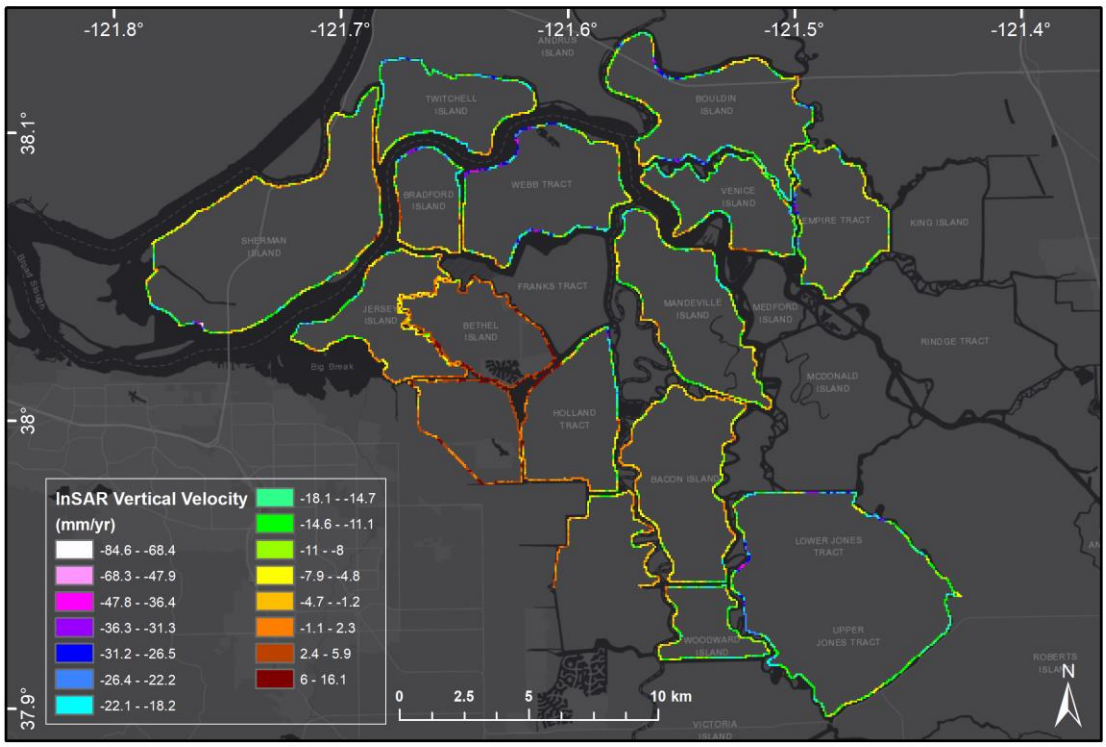

Figure S3. Overview vertical velocity map. Vertical velocity for the central and western Delta islands where blue and purple denote subsidence and orange and red areas show more stable or uplift areas. Pixel size is enlarged to 70 m for better visibility.

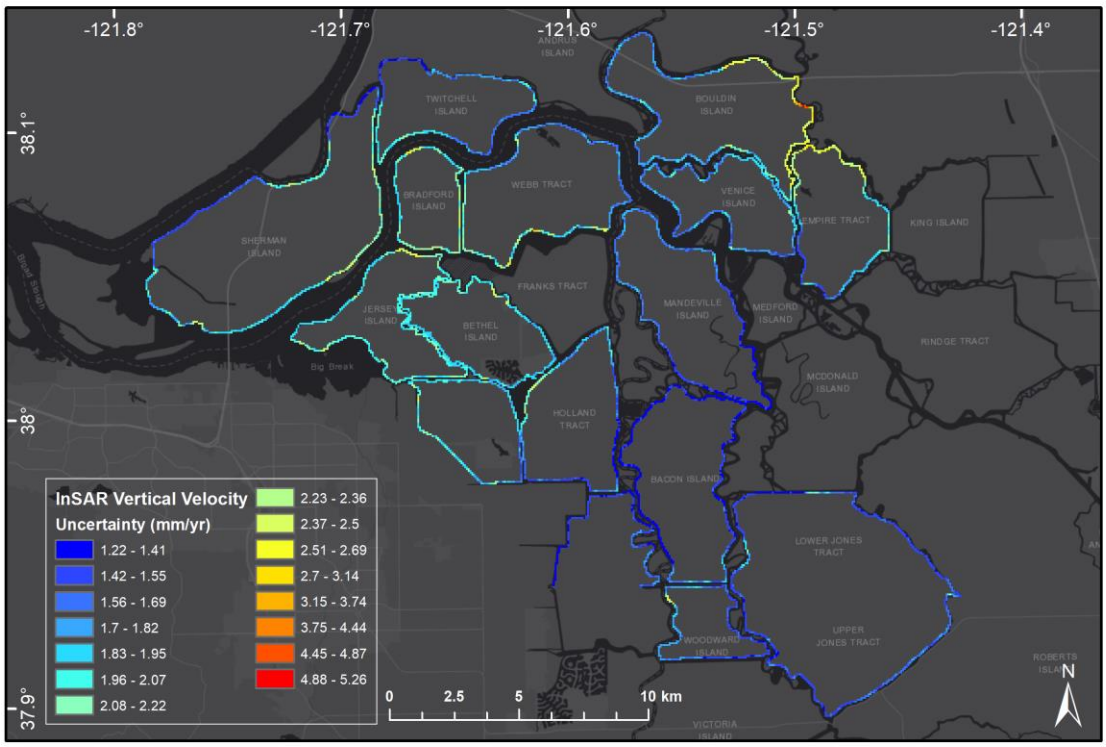

Figure S4. Overview uncertainty map. Vertical velocity uncertainty values for the central and western Delta islands where blue and purple denote lower uncertainty and orange and red areas show more uncertainty. Pixel size is enlarged to 70 m for better visibility.

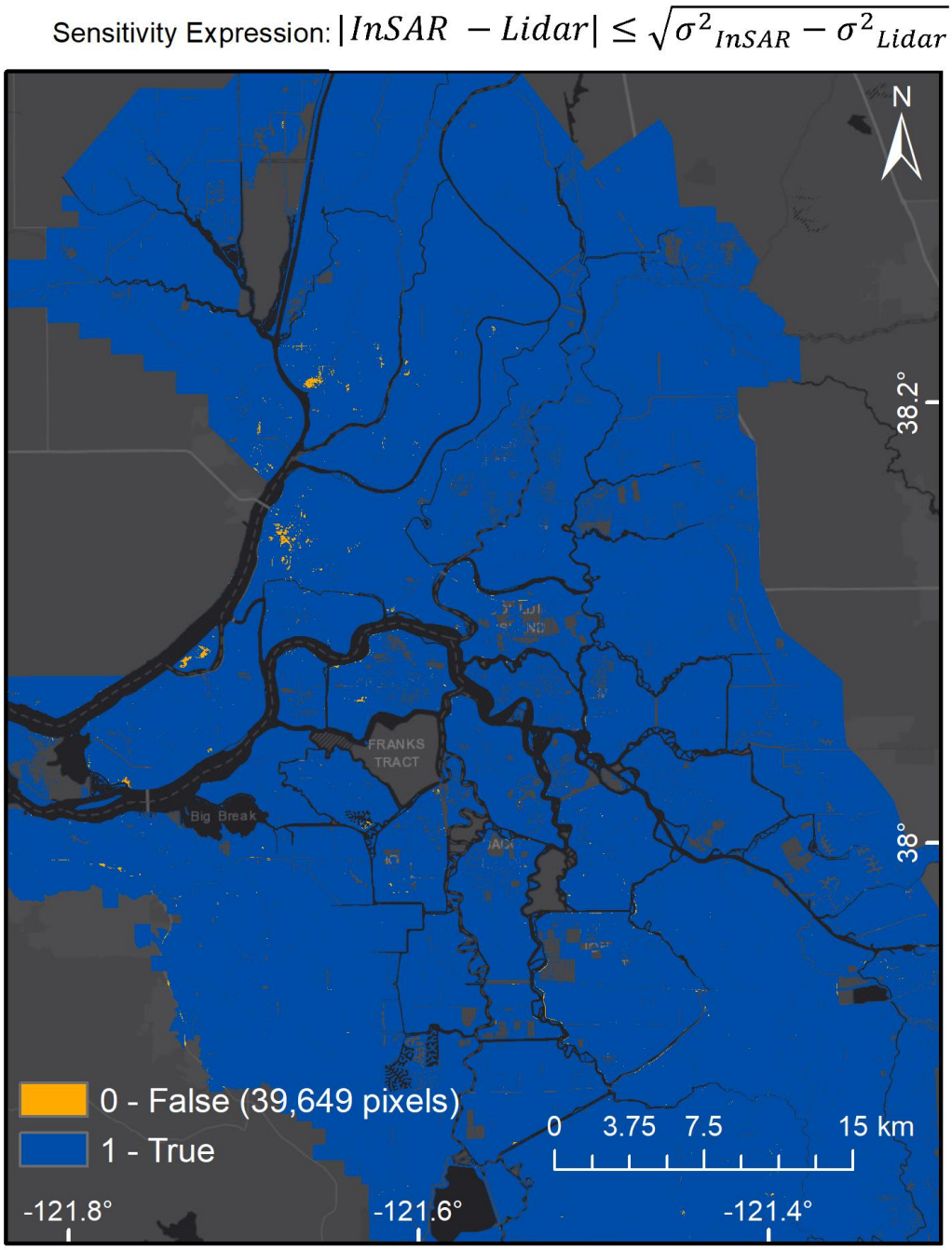

Figure S5. Sensitivity analysis. The sensitivity between the InSAR and lidar datasets was calculated using the above expression, where σ_{InSAR} is the 1-sigma uncertainty calculated for the InSAR vertical velocity rates (see Bekaert, et al. 2019) and σ_{LiDAR} is 10.7 mm/yr, which is the 1-sigma uncertainty as calculated from the 95% confidence level values for vertical accuracy reported from the lidar datasets. Orange pixels show areas where the difference between InSAR and lidar is not within uncertainty bounds, and blue pixels show areas where the datasets are within each other's 1-sigma uncertainty bounds.

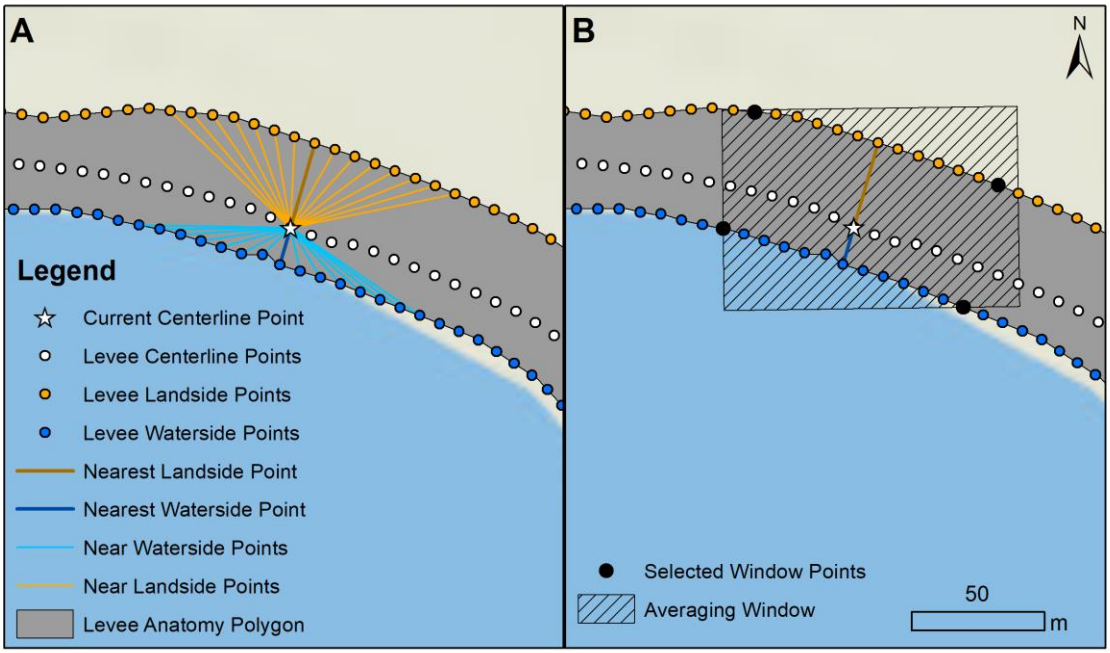

Figure S6. Levee oriented moving window average. (a) An example levee section on southwest Sherman Island showing the levee centerline (white), landside (orange), and waterside (blue) points generated from the levee anatomy polygon (grey). While working on the current centerline point (white star), the nearest landside and waterside points are located. (b) Counting six points away on both sides from the nearest landside and waterside points, the window border points of the averaging window are chosen (black). Based on these window points, a best-fit averaging window is generated.

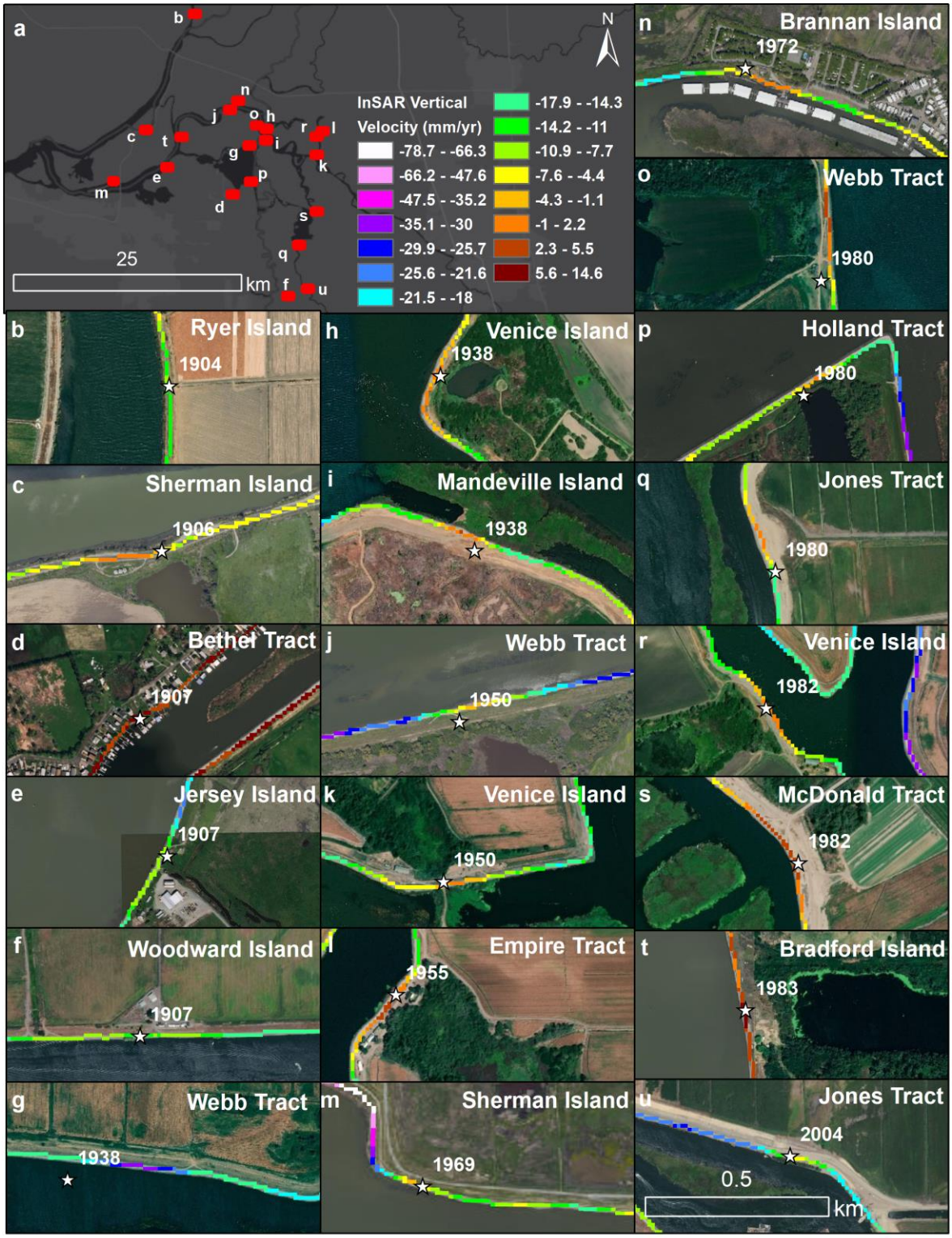

Figure S7. More historic levee breaks. (a) Overview of the Sacramento-San Joaquin Delta with locations of all levee breaks (red). (b-u) Vertical velocities showing more stable conditions at historic levee break throughout the Delta.